

# Acoustic streaming measurements in annular thermoacoustic engines

Stéphane Job<sup>a)</sup>

*Laboratoire d'Acoustique (UMR CNRS 6613), Université du Maine, 72000 Le Mans, France*

Vitalyi Gusev

*Laboratoire de Physique de l'Etat Condensé (UMR CNRS 6087), Laboratoire d'Acoustique (UMR CNRS 6613), Université du Maine, 72000 Le Mans, France*

Pierrick Lotton and Michel Bruneau

*Laboratoire d'Acoustique (UMR CNRS 6613), Université du Maine, 72000 Le Mans, France*

(Received 28 December 2001; revised 23 December 2002; accepted 6 January 2003)

Experiments with an annular thermoacoustic engine employing quasiadiabatic interaction between traveling acoustic waves and an inhomogeneously heated porous material indicate the presence of a closed-loop mass flux. A qualitative modeling of the enthalpy flux in the thermoacoustic core provides an opportunity to estimate the thermal convection associated with this mass flux, by using temperature measurement at different positions in the system. The estimated acoustically induced mass flux is in accordance with recent theoretical results. © 2003 Acoustical Society of America. [DOI: 10.1121/1.1555076]

PACS numbers: 43.35.Ud, 43.25.Zx, 43.20.Mv [MFH]

## I. INTRODUCTION

Thermoacoustic (TA) interaction, the interaction between acoustic waves and temperature oscillations, is a phenomenon developed in acoustic boundary layers near rigid walls.<sup>1</sup> The TA interaction occurring in acoustic resonators subjected to inhomogeneous heating may become unstable and leads to the generation of acoustic oscillations.<sup>1</sup> This effect is enhanced by using the interaction between an inhomogeneously heated stack of solid plates placed in the resonator and the gas oscillations for the transformation of thermal energy into mechanical energy. The idea of a traveling wave annular TA engine was put forward more than 20 years ago.<sup>2</sup> However, the first quasiadiabatic annular TA engine was built only a few years ago.<sup>3</sup> Recently, a closed-loop TA engine which employed quasi-isothermal sound propagation through the stack (Stirling cycle through the regenerator) was reported.<sup>4</sup> This experiment<sup>4</sup> demonstrated that circulation of the gas is induced by the traveling wave in a TA Stirling engine. More recently, the presence of closed-loop induced acoustic streaming has been reported in an annular Stirling cooler driven by a TA regenerator (also called the prime-mover stack in comparison with the cooler stack).<sup>5</sup> This closed-loop mass flux contributes to the enthalpy transport in annular devices, and should be suppressed in order to increase the efficiency of a TA engine.<sup>4,5</sup> The experiments with externally induced mass flux (of nonacoustical nature) through TA stack have been also reported.<sup>6,7</sup> Acoustically induced mass flux has been theoretically predicted in annular Stirling engine.<sup>8</sup> However, neither measurements nor estimates of the acoustically induced streaming mass flux have been reported in an annular acoustic resonator driven by a quasiadiabatic TA prime mover.

In the present paper, results of temperature measurements at some characteristic positions in the quasiadiabatic stack driving an annular acoustic resonator are presented, both above and below the threshold for TA instability. It is demonstrated that, similarly to the case of a TA engine with a quasi-isothermal stack,<sup>4</sup> a closed-loop circulation of the gas is excited in a quasiadiabatic stack. A simple theoretical model provides an estimate of the acoustically induced mass flux. This value matches results from recently developed theory.<sup>9</sup> Theoretical estimation<sup>9</sup> of closed-loop acoustic streaming in annular TA devices can be very helpful, for example, to choose an appropriate working fluid that minimizes acoustically induced mass flux.

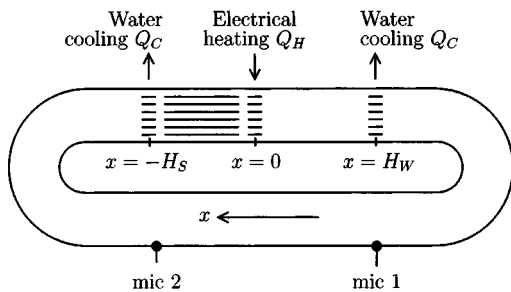
The annular TA engine under study is described in Sec. II and observations of some of acoustical and thermal phenomena are presented. An experimental method to determine the acoustically induced mass flux from temperature measurements is presented in Sec. III. Measured values of this mass flux are compared to the available theoretical estimation<sup>9</sup> and its improvement in Sec. IV before concluding in Sec. V. Improvements of theoretical results presented in Ref. 9 are exposed in the Appendix.

## II. EXPERIMENTAL SETUP: DESCRIPTION AND OBSERVATIONS

The annular TA engine used in our experiments is presented in Fig. 1(a). This resonator, which consists of a torus-shaped waveguide made of stainless-steel (AISI 316L) cylindrical pipes, is composed of two straight pipes (length 0.6 m) and two curved pipes (curvature radius 0.14 m). All pipes have circular cross section (inner radius  $r_i \approx 26.5$  mm, outer radius  $r_o \approx 30.1$  mm, and wall thickness 3.6 mm) and the total axial length of the waveguide is  $L \approx 2.24$  m. This waveguide is filled with air at ambient temperature  $T_0 \approx 293$  K

<sup>a)</sup>Electronic mail: stephane.job@univ-lemans.fr

**(a) Annular thermoacoustic prime-mover**



**(b) Thermoacoustic core**

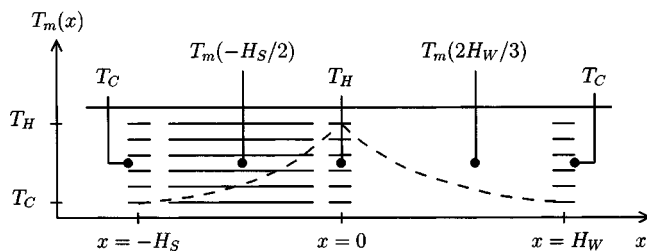


FIG. 1. (a) Schematic view of the annular TA engine ( $L \approx 2.24$  m) and the two piezoresistive microphones (mic. 1 and mic. 2). (b) Enlarged view of the TA core ( $-H_S < x < H_W$ ,  $H_S \approx 0.15$  m and  $H_W \approx 0.38$  m) with the ceramic stack ( $-H_S < x < 0$ ) and five of the six temperature probes. Temperature distribution is schematically represented in dashed line.

and atmospheric pressure  $P_0 \approx 10^5$  Pa. In the following, ambient condition is related to temperature  $T_0$  and pressure  $P_0$ .

Under specific conditions<sup>1,2,10</sup> presented below in more detail, the TA interaction leads to the development of an instability, called the TA instability: an acoustic field can be generated and sustained in the waveguide. Due to the annular geometry of the waveguide, the axial wave number of acoustic oscillations is attempted to be close to axial resonance conditions  $k_n \approx 2n\pi/L$ , where  $n$  is a strictly positive integer. Moreover, if the wave number is lower than the wave number of the first transversal mode ( $k_0 = 1.84/r_i$ ), only plane wave propagates in the cylindrical pipe. Considering dimensions of the experimental setup, one can estimate that the first 24 ( $k_n < k_0$  leads to  $n \leq 24$ ) axial resonance modes propagate in plane wave. Experimentally, the measured frequency of acoustic oscillations is equal to  $f_1 \approx 152$  Hz: it corresponds to the first resonance mode  $k_1 = 2\pi f_1/a_c \approx 2\pi/L$  of the annular pipe, where  $a_c \approx 340$  m/s is the air sound velocity at cold temperature, and acoustic oscillations propagate in plane wave at this frequency.

Above the onset of the TA instability, the presence of acoustic oscillations also induces a mass flux which results from various nonlinear processes.<sup>1,4,6-11</sup> This acoustically induced mass flux produces a closed-loop circulation of the gas around the annular waveguide that carries the enthalpy by forced thermal convection.

The TA interaction occurs near rigid walls inside acoustic boundary layers.<sup>10</sup> A ceramic porous material (length  $H_S \approx 0.15$  m), made of *Cordierite* and usually used in catalytic exhaust pipe, is placed in the waveguide. This ceramic, called the stack, contains a multitude of square cross-section channels (characteristic transversal width  $D_S \approx 0.9$  mm, approximate wall thickness 0.1 mm) parallel to the waveguide

axis. The stack is used to increase locally the volume of boundary layer in the fluid. Considering that the thermal boundary layer ( $\delta_\kappa = \sqrt{2\kappa/\omega_1} \approx 0.21$  mm) is more than four times smaller than the characteristic transversal width  $D_S$ , TA interaction employs a quasiadiabatic regime<sup>10</sup> ( $\kappa \approx 2.1 \cdot 10^{-5}$  m<sup>2</sup>/s is the thermal diffusivity in air at ambient condition, and  $\omega_1 = 2\pi f_1$  is the angular frequency).

A temperature difference is imposed between stack ends: its left side ( $x = -H_S$ ) is maintained at cold temperature  $T_C = T_0$  and its right side ( $x = 0$ ) is maintained at hot temperature  $T_H > T_C$ . The origin of axial coordinate  $x$  is chosen to be the position of hot temperature  $T_H$ , and the axial coordinate is directed clockwise in Fig. 1(a). Spatial extent of the inhomogeneously heated part of the waveguide ( $0 < x < H_W$ , where  $H_W \approx 0.38$  m) is controlled by imposing the cold temperature  $T_C$  at the position  $x = H_W$ . The inhomogeneously heated region  $-H_S < x < H_W$ , presented in Fig. 1(b), is called the TA core. The heated region of the stack is denoted by the subscript  $S$ , and the heated region of the waveguide by the subscript  $W$ .

Temperatures at cold positions ( $x = -H_S$  and  $x = H_W$ ) are imposed by using two cold heat reservoirs (at cold temperature  $T_C$ ), which consist of two water-cooled copper shells set around the waveguide. Two cold heat exchangers made of copper wire grids (wire approximately 0.2 mm in diameter and approximately 1 mm spaced) are placed in contact with cold reservoirs perpendicularly to the waveguide axis. One of the heat exchangers ( $x = -H_S$ ) is in contact with the stack. Copper grids, ensuring a uniform radial temperature distribution in the cross section of the pipe, are designed to achieve approximately the same characteristic transversal width as in the stack.

A hot heat reservoir (temperature  $T_H$  at position  $x = 0$ ), consisting of eight electrical cartridges (125 W each) soldered in a stainless-steel block, is placed in contact with external surface of the waveguide. The electrical power  $Q_H$  supplied to the hot heat reservoir is extracted by measuring electrical voltage and current supplied to the cartridges. A hot heat exchanger is placed in contact with the stack, in front of the hot heat reservoir, and firmly in contact with internal surface of the waveguide. The hot heat exchanger is an appropriately coiled stainless-steel ribbon (width 2.5 cm and thickness 10  $\mu$ m). The distance between two adjacent walls in the hot heat exchanger, chosen to be close to the characteristic transversal width in the stack, is approximately 1 mm.

When an axial distribution of the mean temperature  $T_C < T_m(x) < T_H$  of the fluid is imposed in the TA core ( $-H_S < x < H_W$ ), the TA interaction can be seen from a simplified point of view as the conversion of a part of the supplied heat in mechanical energy of acoustic oscillations.<sup>10</sup> The TA interaction mainly occurs in the stack. This interaction leads to the amplification of an acoustic wave traveling through the stack in the direction of positive temperature gradient.<sup>1,2,10</sup> When the ratio  $T_H/T_C$  of hot to cold temperature reaches the threshold value  $(T_H/T_C)_{th} \approx 1.9$ , the TA amplification in the stack compensates acoustic dissipation in the waveguide and the system becomes unstable. Any initial acoustical perturbation (noise for example) is first amplified at resonance fre-

quency and then sustained in the waveguide. The threshold condition is achieved by applying an electrical load of  $Q_{th} \approx 130$  W.

Considering that acoustic oscillations propagate in plane waves, the acoustic field can be expressed in the form  $p(x,t) = \text{Re}[\tilde{p}(x)e^{-i\omega_1 t}]$ , where

$$\tilde{p}(x) = [\tilde{p}^+(x_0)e^{+ik_W(x-x_0)} + \tilde{p}^-(x_0)e^{-ik_W(x-x_0)}] \quad (1)$$

is the acoustic pressure in frequency domain. The acoustic wave number  $k_W$ , which takes into account dissipative and dispersive effects in the cold part of the waveguide, is defined as

$$k_W \approx k_C [1 + (1+i)c(\delta_\nu/r)]. \quad (2)$$

In Eq. (2),  $k_C = \omega_1/a_C$  is the acoustic wave number at cold temperature in absence of sound interaction with walls,  $\delta_\nu = \sqrt{2\nu/\omega_1} \approx 0.17$  mm is the viscous boundary layer,  $\nu \approx 1.5 \cdot 10^{-5}$  m<sup>2</sup>/s is the kinematic viscosity in air at ambient condition,  $c = (1/2)[1 + (\gamma-1)/\sqrt{\sigma}] \approx 0.74$  is the Kirchhoff's constant,<sup>1,12</sup>  $\gamma \approx 1.4$  is the polytropic coefficient, and  $\sigma = \nu/\kappa \approx 0.71$  is the Prandtl number of air.

Two piezoresistive PCB microphones placed at  $x_{m1} \approx 0.95$  m and  $x_{m2} \approx 1.53$  m allow the measurement of the acoustic field. Each microphone has been calibrated in phase and in amplitude by comparison with a reference B&K microphone. By measuring acoustic pressure at two separated positions  $x = x_{m1}$  and  $x = x_{m2}$ , one can extract frequency of acoustic oscillations and both contrapropagating wave complex amplitudes  $\tilde{p}^+(x_0)$  and  $\tilde{p}^-(x_0)$  anywhere in the cold part of the waveguide ( $x_0 < -H_S$  or  $x_0 > H_W$ ). Clockwise and anticlockwise traveling waves amplitudes  $\tilde{p}^+(-H_S) \equiv p^+$  are then extracted as a function of heat supplied  $Q_H$ . As shown in Fig. 2(a), the acoustic pressure amplitude increases when heat load  $Q_H$  is increased above the TA instability threshold condition. It is estimated that the amplitude of the clockwise-traveling wave  $|\tilde{p}^+|$  exceeds the amplitude of the wave traveling in the opposite direction  $|\tilde{p}^-|$  by more than a factor of 2, as shown in Fig. 2(b). However, the amplitude of the anticlockwise traveling wave is not completely negligible. This can be explained by the fact that though only the clockwise-traveling wave is amplified in the heated stack,<sup>1,2,10</sup> a significant part of this wave is reflected in the system. Relative phase  $\phi(p^-/p^+) = \phi(p^-) - \phi(p^+)$  measurements, also presented in Fig. 2(b), confirm that the interaction between contrapropagating waves in the annular TA resonator is not trivial: the acoustic field generated in the system is neither a standing wave nor a purely traveling wave acoustic field.<sup>3,5</sup>

Temperature measurements are obtained by using six thermocouples (1 mm in diameter type-K probes). Five of them are set in the TA core ( $x = -H_S$ ,  $-H_S/2$ ,  $0$ ,  $2H_W/3$ ,  $H_W$ ) on the axis of the waveguide as shown in Fig. 1(b). The two cold thermocouples ( $x = -H_S, H_W$ ) are placed in contact with the two cold heat exchangers outside the TA core. The hot temperature thermocouple ( $x = 0$ ) measures the temperature at the center of the hot heat exchanger. The sixth temperature probe (not shown in Fig. 1) controls that the temperature far outside the TA core (in the cold part of the waveguide) remains constant (i.e., at cold temperature  $T_C$ ).

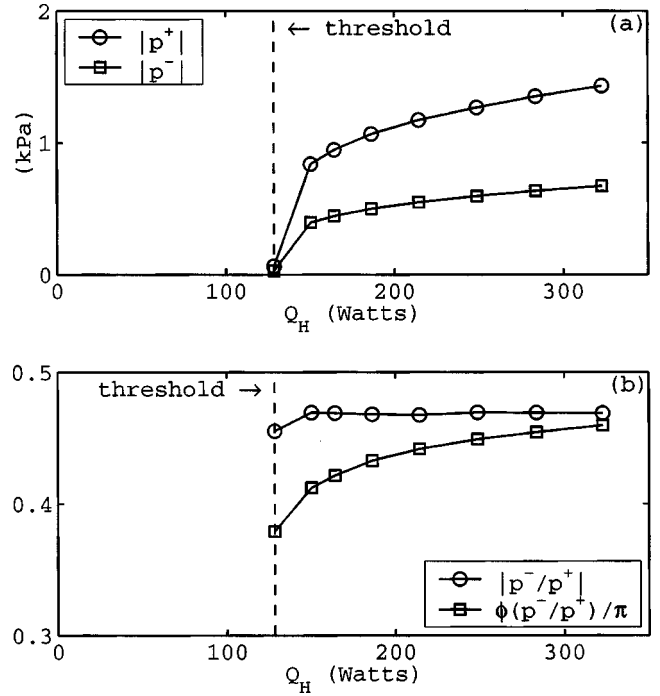


FIG. 2. (a) Measured amplitudes of clockwise ( $\tilde{p}^+$ ) and anticlockwise ( $\tilde{p}^-$ ) waves, plotted versus heat load  $Q_H$ . (b) Modulus and phase of the ratio  $R(-H_S) = \tilde{p}^-/\tilde{p}^+$  plotted versus heat load  $Q_H$ . Instability onset occurs at  $Q_H \approx 130$  W.

The six thermocouples used are provided from the same manufacturing series and are certified by the manufacturer. It has been checked that all thermocouples give the same measurement (within an error of less than 1 K) of the ambient temperature  $T_0$ . As a consequence, absolute temperature measurement may be considered within an error of the order of 1 K. Despite this accuracy, the relative error in absolute temperature measurements is overestimated to  $\pm 5\%$ . In the whole range of experiments, this relative error corresponds at least to  $\pm 15$  K (at ambient temperature  $T_0$ ) and at the most to  $\pm 30$  K (at the highest measured temperature), which is much greater than the usual accuracy of type-K probes (less than 1 K). This overestimation of the error in temperature measurement is introduced to take into account the lack of other sources of errors. For example, it is assumed in the following that the temperature does not depend on radial coordinate, although it may vary in the cross section of the waveguide. In fact, this variation is less than or equal to 3 K,<sup>13</sup> i.e., less than the considered relative error of  $\pm 5\%$  in temperature measurement.

Results of temperature measurements are presented in Fig. 3, below and above the onset of TA instability. As shown in Fig. 3(a), where absolute temperature measurements are plotted as functions of the heat load  $Q_H$ , it is first checked that cold temperature  $T_C$  (measured outside the TA core) and cold exchangers temperatures  $T_m(-H_S)$  and  $T_m(H_W)$  (not shown in Fig. 3) remain constant and equal to ambient temperature  $T_0$  in the whole range of experiments. It is then noted that below the threshold condition, hot temperature  $T_H$ , temperature measured at  $x = -H_S/2$  (in the stack), and temperature measured at  $x = 2H_W/3$  (in the heated part of the waveguide) increase when  $Q_H$  increases. At the threshold

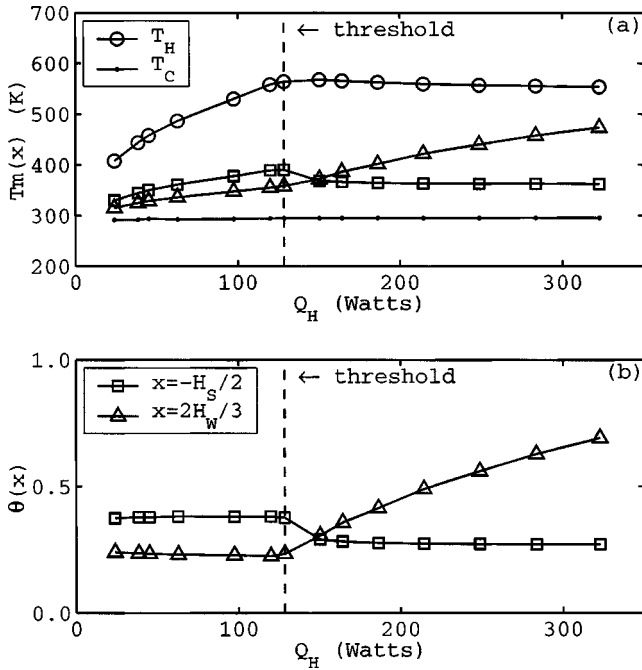


FIG. 3. (a) Absolute measured temperatures above and below the threshold condition for TA instability onset plotted vs heat load  $Q_H$ . (b) Normalized temperatures  $\theta(x) = [T_m(x) - T_C] / [T_H - T_C]$  calculated from inset (a). In inset (a), circles are hot temperature measurements ( $x=0$ ) and dots are cold temperature measurements (far outside the TA core). In inset (a) and (b), squares are temperatures measured inside the stack ( $x = -H_S/2$ ) and triangles are temperatures measured inside the heated part of the waveguide ( $x = 2H_W/3$ ). Error bounds in temperature measurements are not shown.

condition, acoustical phenomena (i.e., acoustic waves and acoustically induced mass flux) are generated: the thermal behavior of the system is modified. Above the threshold, temperature  $T_H$  remains approximately constant whereas  $Q_H$  increases, and an evolution of the temperature profile in the TA core is observed. This demonstrates that there is a significant influence of streaming on temperature distribution: the thermal forced convection led by the acoustically induced mass flux transports cold air from the cold part of the waveguide through the TA core.

Temperature profile evolution in the TA core is described in Fig. 3(b) by using a normalized temperature defined in the form

$$\theta(x) = [T_m(x) - T_C] / [T_H - T_C]. \quad (3)$$

The latter quantity  $\theta(x)$  is also used in the thermal model presented in Sec. III. The normalized temperature  $\theta(x)$  is evaluated at characteristic positions  $x = -H_S/2$  and  $x = 2H_W/3$  and plotted in Fig. 3(b) as a function of heat load  $Q_H$ . The decreasing of the normalized temperature  $\theta(x)$  at  $x = -H_S/2$  and its increasing at  $x = 2H_W/3$  indicate that a mass flux carrying the enthalpy parallel to the waveguide axis is induced above the threshold of the TA instability. Moreover, the direction of the bend indicates that the mass flux is directed toward the clockwise direction. The fact that the direction of the mass flux is the same as the direction of the amplified traveling wave is in accordance with available theoretical results for annular TA engines driven by quasidiabatic prime mover.<sup>9</sup>

### III. MASS FLUX MEASUREMENT

In order to measure the mass flux, the following qualitative model of the axial temperature distribution in the TA core is proposed. The aim of this model is to provide an estimation of the order of magnitude of the acoustically induced mass flux. It is not intended to ensure accurate quantitative measurements. In the frame of this approach, simplifying assumptions have been used. The temperature distribution inside the cylindrical tube is assumed to be independent of the radial coordinate. This assumption has been confirmed experimentally<sup>13</sup> by using additional thermocouples (thinner and more sensitive than actual temperature probes) in the radial direction of the stack. The temperature variation in the cross section is less than or equal to 3 K.<sup>13</sup> Neglecting radial contributions, the enthalpy flux can be written in the form

$$J = -A \partial_x T_m + C_p M T_m, \quad (4)$$

where  $\partial_x \equiv \partial / \partial x$  denotes the partial  $x$  derivative,  $C_p \approx 10^3$  J/(kg K) the specific heat of air,  $M$  the mass flux (expressed in kg/s) averaged over the cross section of the waveguide, and  $A$  a constant. The second term in the right-hand side (r.h.s.) of Eq. (4) takes into account the forced thermal convection due to the mass flux  $M$ . The first term in the r.h.s. of Eq. (4) describes the thermal conduction, so the constant  $A$  can be considered as an area scaled effective thermal conductivity

$$A \equiv k_{st} \pi (r_o^2 - r_i^2) + k_{air} \phi \pi r_i^2 + k_{ce} (1 - \phi) \pi r_i^2, \quad (5)$$

where  $k_{st} \approx 16$  W/(m K) at  $T \approx 373$  K and  $k_{st} \approx 25$  W/(m K) at  $T \approx 973$  K (intermediate values are obtained using a linear fit),  $k_{air} \approx 0.025$  W/(m K), and  $k_{ce} \approx 1$  W/(m K) are, respectively, the thermal conductivities of steel, air, and ceramic. In the frame of our qualitative approach,  $C_p$ ,  $k_{air}$ , and  $k_{ce}$  are assumed to be temperature-independent constants. The porosity (the volume of fluid divided by the total volume of the stack region) is taken equal to  $\phi \approx 0.8$  in the region  $-H_S < x < 0$  and to  $\phi = 1$  in the region  $0 < x < H_W$ .

The heat transfer from the external surface of the waveguide to the surroundings is modeled by using the Newton's law of cooling:<sup>14</sup>

$$\partial_x J + h(T_m - T_C) = 0, \quad (6)$$

where  $h$  is a phenomenological coefficient of heat transfer (mainly due to natural convection and radiation). The first term of the left-hand side (l.h.s.) of Eq. (6) describes the axial variation of the enthalpy flux caused by heat leakage to surroundings in radial direction (second term of l.h.s.). Finally, substituting Eq. (4) into Eq. (6), an equation for the temperature distribution is obtained

$$A \partial_{xx}^2 \theta - C_p M \partial_x \theta - h \theta = 0, \quad (7)$$

where  $\theta(x)$  is the normalized mean temperature of the fluid defined in Eq. (3).

In order to find a tractable analytical solution, coefficients in Eq. (7) (which in fact all depend on temperature) are approximated by their mean values, estimated at a characteristic temperature  $T_{char} = (T_H + T_C) / 2$ . In the frame of our qualitative thermal model, coefficients in Eq. (7) are thus

assumed to be independent of the local temperature and consequently independent of the spatial coordinate. For an imposed temperature  $T_H$ , it is then straightforward to find the solution (depending on position  $x$  and on parameter  $h$  and  $M$ ) of the linear differential equation Eq. (7) with constant coefficients. This solution satisfies the boundary conditions  $\theta(x=0)=1$ ,  $\theta(x=-H_S, H_W)=0$ , both in the stack region ( $-H_S < x < 0$ ) and in the waveguide region ( $0 < x < H_W$ ). Consequently, if coefficients  $A$  and  $h$  are known, mass flux  $M$  can be extracted by mapping the solution to Eq. (7) to temperature measurements.

It is important to keep in mind that in the frame of our one-dimensional thermal theory, the quantity  $M$  involved in Eq. (7) is the acoustically induced mass flux averaged over the cross section of the waveguide. However, the mass flux actually depends on the radial coordinate in the form of a parabolic laminar flow:<sup>9,15</sup>  $M(r) \approx M(r=0)[1 - (r/r_i)^2]$ . Assuming the expected velocity of the streaming<sup>9</sup> is of the order of magnitude of  $v \sim 10^{-2}$  m/s and using the thermal diffusivity of air ( $\kappa \approx 2.1 \cdot 10^{-5}$  m<sup>2</sup>/s), the characteristic distance of thermocouple sensitivity is of the order of  $\kappa/v \sim 2$  mm  $\ll r_i$ . Temperature measurements at  $r=0$  thus provide the local measurement  $M(r=0)$  of the mass flux, and the correct value of the mass flux averaged over the cross section of the waveguide is equal to  $M(r=0)/2$ .

It is interesting to analyze the order of magnitude of involved thermal effects. First, the thermal conduction in the steel wall of the pipe [first term in the r.h.s. of Eq. (5)] is approximately 100 times greater than thermal conduction in air or in ceramic stack [second and third terms in the r.h.s. of Eq. (5)]. Second, in the whole range of our experiments, it has been checked that thermal conduction [first term in the l.h.s. of Eq. (7)] and heat leaks [third term in the l.h.s. of Eq. (7)] are of the same order of magnitude. Third, above the threshold condition (when a mass flux is generated), it has been checked that the forced convection [second term in the l.h.s. of Eq. (7)] is at least twice greater (for the minimum value of the mass flux measured near the threshold condition) and at the most ten times greater (for the maximum measured mass flux) than both other contributions [first or third terms in the l.h.s. of Eq. (7)]. Thereby, forced thermal convection due to the mass flux  $M$  is the dominant effect described in Eq. (7).

Although the mass flux depends on the radial coordinate (in the form of a parabolic laminar flow), the enthalpy flux carried by the forced thermal convection is only directed toward the axial coordinate. Similarly, because of the high thermal conductivity of steel, and because temperature gradients are only imposed in the axial direction, radial temperature gradients in the wall of the pipe are weak. Enthalpy flux carried by thermal conduction in steel is negligible in the radial direction compared to its contribution in the axial direction. Moreover, thermal conduction in air and in ceramic is negligible both in the axial and in the radial direction compared to axial thermal conduction in steel and thermal forced convection in the gas. Finally, except for heat leaks from external surface of the waveguide to the surroundings [Eq. (6)], thermal contributions in radial direction

do not have significant influence on temperature distribution and can be neglected in Eq. (4).

The following procedure is applied to evaluate the mass flux  $M$ . First, phenomenological parameters  $h_S$  and  $h_W$  are measured. For this purpose, an absorbing partition is installed in the cold part of the waveguide in order to prevent the TA instability. Thus,  $M \equiv 0$  and by mapping the solutions of Eq. (7), respectively, to the measured values of the temperature at  $x = -H_S/2$  and  $x = 2H_W/2$ , values of coefficients  $h_S$  and  $h_W$  are found as a function of  $T_{\text{char}}$ . It appears that both these coefficients weakly depend on the characteristic temperature. Orders of magnitude of these coefficients are  $h_S \sim 1.4$  W/(m k) and  $h_W \sim 0.3$  W/(m K) at ambient temperature, and they vary no more than 10% in the whole range of our experiments. Second, the absorbing partition is removed to allow the TA instability development. By mapping the theoretical solution of Eq. (7) to the experimental temperature measured at  $x = 2H_W/3$  above the threshold, and by using previous measurements of  $h_W$  (as a function of  $T_{\text{char}}$ , i.e., as a function of  $Q_H$ ) the dependence of the mass flux  $M$  on the supplied heat  $Q_H$  can be extracted.

The mass flux  $M$  and the coefficients  $h_S$  and  $h_W$  being known, theoretical temperature distributions satisfying Eq. (7) can be evaluated. Two examples of theoretical fit of the axial temperature distribution are given in Fig. 4, where circles represent measured values. Solid line and dashed line in Fig. 4 represent mapped solutions of Eq. (7) to temperatures, respectively, measured above and below the threshold condition for TA instability. The bending of the temperature curve above threshold condition indicates the presence of the mass flux carrying enthalpy parallel to the waveguide axis in a clockwise direction.

Finally, the use of mass flux measurements as function of  $Q_H$  and the use of acoustic wave amplitude measurements as functions of  $Q_H$  (see Fig. 2), provide the dependence of  $M$  as a function of  $|\tilde{p}^+|$ , for example. The acoustically induced mass flux per unit area  $M/(\pi r_i^2)$  (mass flux  $M$  normalized to the cross-section area  $\pi r_i^2$  of the pipe) is plotted as a function of  $|\tilde{p}^+|^2$  in Fig. 5, where circles are measured values. Error bounds in Fig. 5 correspond to minimal and maximal values of the mass flux obtained from the latter mapping process, when the  $\pm 5\%$  relative error is applied to measured values of all temperatures.

#### IV. MASS FLUX THEORETICAL PREDICTION

In a previous paper,<sup>9</sup> a theory was proposed to predict the acoustically induced mass flux in an annular TA engine. The purpose of this paper was to find the dominant physical behavior of the acoustically induced mass flux. First, the stack was assumed to be acoustically thin (the dimensionless parameter  $\mu \equiv k_c H_S \ll 1$  was supposed to be small). Second, the porosity was set equal to one ( $\phi = 1$ ). From an experimental point of view, these assumptions appear too constraining (experimentally:  $\mu \approx 0.42$  and  $\phi \approx 0.8$ ). In order to take into account these experimental constraints, an improvement of the previous theory<sup>9</sup> is proposed in the Appendix. Furthermore, another improvement should be considered concerning the contribution of the anticlockwise traveling

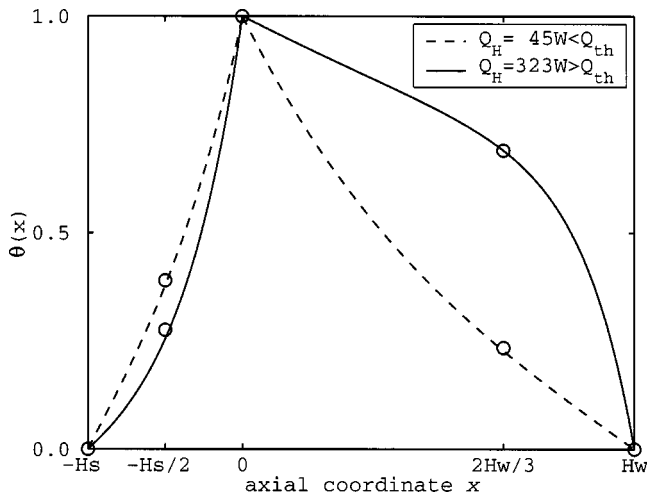


FIG. 4. Two examples of axial temperature distribution  $\theta(x)$  in the TA core, below (dashed line  $Q_H \approx 45$  W) and above (solid line  $Q_H \approx 323$  W) the threshold condition ( $Q_{th} \approx 130$  W). Curves are calculated using solution of Eq. (7), where constant  $A$  is known, coefficients  $h_S$  and  $h_W$  are determined from temperature measurements below the onset (respectively, at  $x = -H_S/2$  and  $x = 2H_W/3$  when  $M=0$ ), and the mass flux  $M$  is extracted below the onset from temperature measurements at  $x = 2H_W/3$ . Circles are measured values, error bounds being not shown.

wave. Although the measured ratio of contrapropagating waves  $|R| \equiv |\tilde{p}^-/\tilde{p}^+| \approx 0.47$  is not negligible, the influence of the anticlockwise wave was not analyzed in the model described in Ref. 9.

In accordance with the theory<sup>9</sup> and the Appendix, terms proportional to the thickness  $\mu \ll 1$  of the stack are first neglected (porosity  $\phi \approx 0.8$  is taken into account). The theoretical expression for the acoustically induced mass flux per unit area can be derived in the form of Eq. (A14)

$$M_0 \approx \Delta |\tilde{p}^+|^2. \quad (8)$$

From Eq. (8), the predicted mass flux  $M_0$  is proportional to the square of acoustic pressure amplitude, where the proportionality coefficient  $\Delta$  is given by

$$\Delta = \left( \frac{2/\phi}{2.37} \right) \frac{(c+d/2)}{12\pi\rho_C a_C^3} \left( \frac{D_S}{\delta_\nu} \right) \left( \frac{L}{H_S} \right) \left( \frac{\beta+1}{\beta-1} \right) \times \frac{[(T_H/T_C)^{(\beta-1)/2} - 1]}{H_S^{-1} \int_{-H_S}^0 dx T_N^{\beta+1}(x)}. \quad (9)$$

The density of air at cold temperature is  $\rho_C \approx 1.2$  kg/m<sup>3</sup>. The phenomenological parameter  $\beta \approx 0.73$ <sup>1,12</sup> takes into account that kinematic viscosity and thermal diffusivity of air depend on temperature:  $\nu \propto \kappa \propto T_m^{\beta+1}(x)$ . The coefficient  $d = (1/\sqrt{\sigma})[2/(1+\beta)/(1+\sqrt{\sigma}) - (\gamma-1)] \approx 0.28$  is the Kramer's constant.<sup>1,12</sup>

An improvement of the theory is achieved by considering correction terms proportional to the thickness  $\mu$  of the stack. The mass flux is obtained in the form of Eq. (A17)

$$M_1 \approx (\Delta + \Delta') |\tilde{p}^+|^2, \quad (10)$$

where the additional coefficient  $\Delta'$  is:

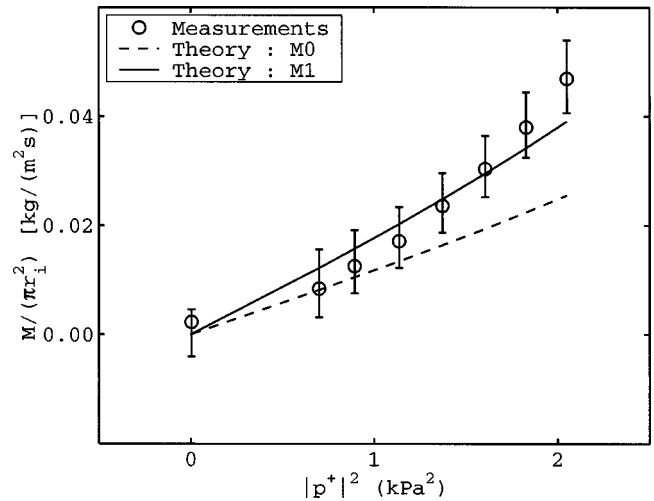


FIG. 5. Acoustically induced mass flux normalized to the cross section of the waveguide  $M/(\pi r_i^2)$  plotted versus square of the clockwise traveling wave measured amplitude  $|\tilde{p}^+|^2$ . Circles with error bounds are estimated values from temperature measurements. Lines are the theoretical estimations given in Sec. IV. The dashed line is the lowest approximation  $M_0$  of the mass flux induced by the clockwise acoustic wave. The solid line corresponds to the improved approximation  $M_1$  of the acoustically induced mass flux.

$$\Delta' = \left( \frac{2}{2.37} \right) \frac{(3-2c)}{6\rho_C a_C^3} \left( \frac{D_S}{\delta_\nu} \right) \frac{\int_{-H_S}^0 dx T_N^{[(\beta-1)/2]}(x)}{\int_{-H_S}^0 dx T_N^{\beta+1}(x)}. \quad (11)$$

Theoretical estimates of mass fluxes  $M_0$  and  $M_1$  are plotted as functions of  $|\tilde{p}^+|^2$  and compared to measured value in Fig. 5. Orders of magnitude of experimental and theoretical estimates are in a satisfactory agreement, the most important finding being that the acoustically induced mass flux dependence on acoustic wave amplitude  $|\tilde{p}^+|$ , which is close to quadratic, has been experimentally demonstrated. The lowest approximation  $M_0$  of the theoretical acoustically induced mass flux appears to be insufficient to fit experimental data. In contrast, the improved theoretical prediction  $M_1$  obtained by considering correction terms proportional to the thickness of the stack is in a better agreement with experimental data. Nevertheless, the influence of the anticlockwise wave has been neglected: this can explain why the predicted mass flux  $M_1$  is still slightly lower than the experimental finding at high acoustic pressure amplitude.

Thus, it can be concluded that the qualitative thermal model presented in this paper provides a reasonable explanation for the experimental observations. It should be mentioned that in the region between the heat exchangers there also exists additional acoustic streaming that does not contribute to the cross-sectional average mass flux but may participate in the heat transport.<sup>4</sup> Our experimental findings and their interpretation demonstrate that in the system under consideration this additional acoustic streaming contribution to heat transfer between the heat exchangers is not significant. This correlates with our theoretical estimates based on the theory of the Rayleigh-type streaming.<sup>11,16</sup> It is predicted that, even though in our experiments the characteristic velocity of this streaming is of the order of  $M/(\pi r_i^2)/\rho_C$ , the enthalpy flux carried by this streaming is nevertheless at least

two orders of magnitude weaker than the one carried by the annular streaming. There are two reasons for this. First, the Rayleigh-type streaming velocity near the walls of the tube and near the axis of the waveguide are in opposite directions. The enthalpy flux is significantly canceled in the cross section and  $M=0$ . Second, the measured radial temperature gradients<sup>13</sup> are estimated to be small in our experiments.

## V. CONCLUSION

The acoustically induced mass flux in the annular thermoacoustic engine using quasiadiabatic stack, found to be in the range of 0.01 kg/(m<sup>2</sup> s) to 0.05 kg/(m<sup>2</sup> s), matches recent theoretical results<sup>9</sup> and their improvements. This needs to be included in modeling annular thermoacoustic engines and should be taken into account in the optimization of thermoacoustic devices.

## ACKNOWLEDGMENTS

The authors are indebted to E. Egon for technical contribution. This work was supported by the Délégation Générale de l'Armement (DGA) under Contract No. 99.34.072/DSP and through the DGA-CNRS Ph.D. fellowship of the first author (S. Job).

## APPENDIX: IMPROVED THEORY OF ACOUSTIC STREAMING IN ANNULAR THERMOACOUSTIC ENGINES

According to recent theoretical results<sup>9</sup> devoted to the study of an annular TA engine driven by a stack composed of parallel plates, the acoustically induced mass flux is expressed in terms of a density of streaming source divided by a hydrodynamic resistance. Dominant contributions of both these quantities are due to the stack. For a stack composed of parallel plates spaced by the distance  $D_S$ , the acoustically induced mass flux per unit area is given by

$$M \simeq \left[ \int_{-H_S}^0 dx s(x) \right] / \left[ (2/D_S)^2 \int_{-H_S}^0 dx \nu_m(x) \right], \quad (\text{A1})$$

where  $\nu_m(x) \propto T_m^{(\beta+1)}(x)$  is the kinematic viscosity at temperature  $T_m(x)$ . The denominator represents the hydrodynamic resistance. The density of streaming source  $s(x)$  is found by substituting Eq. (20) in Eq. (17) of Ref. 9. In the quasiadiabatic regime,  $f_\nu \simeq (1+i)[\delta_\nu/D_S]$  and  $D_S \gg \delta_\nu$ . Considering terms proportional to  $|f_\nu|$ , the density of streaming source is given by

$$s(x) = \frac{1}{6\omega^2\rho_m} \text{Re} [ T_N^{-1} \partial_x T_N |\partial_x \tilde{p}|^2 + \partial_{xx}^2 \tilde{p} \partial_x \tilde{p}^* + k_C^2 T_N^{-1} \tilde{p} \partial_x \tilde{p}^* (1 - 3f_\nu^*) ] + o(|f_\nu|), \quad (\text{A2})$$

where  $T_N \equiv T_m/T_C$  is a normalized temperature and  $\rho_m \propto 1/T_N$  is the density of the fluid. The quantity  $f_\nu \propto T_m^{(\beta+1)/2}$  depends on the temperature and consequently on the position  $x$ . The dependence of  $\tilde{p}(x)$ ,  $T_N(x)$ ,  $\rho_m(x)$ , and  $f_\nu(x)$  on  $x$  is taken into account but has been omitted in Eq. (A2) to simplify the expression.

For a stack composed of square channels (transversal width  $D_S$ ), the volume of the boundary layers in the quasiadiabatic regime is approximately twice compared to a stack of parallel plates, and the hydrodynamic resistance is 2.37 greater.<sup>17</sup> The mass flux per unit area induced in a stack of square channels is then

$$M_{\text{square}} \simeq (2/2.37) M_{\text{plates}}. \quad (\text{A3})$$

It is now necessary to find the axial dependence of the acoustic field  $\tilde{p}(x)$ . In the quasiadiabatic regime, the acoustic wave propagation equation<sup>1,9,10,12</sup> is

$$\partial_{xx}^2 \tilde{p} + [1 - (1/2)(\beta+1)(2c+d)f_\nu] T_N^{-1} \partial_x T_N \partial_x \tilde{p} + k_C^2 T_N^{-1} (1 + 2cf_\nu) \tilde{p} = 0 + o(|f_\nu|), \quad (\text{A4})$$

where  $c$  and  $d$  are, respectively, the Kirchoff's and the Kramer's constants.<sup>1,12</sup> The acoustic field in the stack region is sought in the same way as in Ref. 12. Equation (A4) is rewritten by neglecting contributions proportional to  $|f_\nu| \ll 1$ , that is

$$\partial_x [ T_N \partial_x \tilde{p} ] = -k_C^2 \tilde{p} + o(|f_\nu|^0). \quad (\text{A5})$$

Equation (A5) is then integrated over  $x$ , leading to

$$T_N(x) \partial_x \tilde{p}(x) = T_N(x_0) \partial_x \tilde{p}(x_0) - k_C^2 \int_{x_0}^x dx_1 \tilde{p}(x_1) + o(|f_\nu|^0), \quad (\text{A6})$$

and, once again, Eq. (A6) is integrated over  $x$ , giving

$$\tilde{p}(x) = \tilde{p}(x_0) + \partial_x \tilde{p}(x_0) \int_{x_0}^x dx_1 \frac{T_N(x_0)}{T_N(x_1)} - k_C^2 \int_{x_0}^x \frac{dx_1}{T_N(x_1)} \int_{x_0}^{x_1} dx_2 \tilde{p}(x_2) + o(|f_\nu|^0). \quad (\text{A7})$$

Choosing  $x_0 \equiv -H_S$ , the temperature  $T_N(x_0)$  reduces to  $T_N(-H_S) = 1$ . Each integration over  $-H_S < x < 0$  introduces a correction of the order of  $\mu$ . The first integral in the r.h.s. of Eq. (A6) introduces a correction of the order  $\mu$ , while the first term of the r.h.s. is of the order of  $\mu^0$ . Equation (A7) is an integral formulation of the differential Eq. (A4). The first term of the r.h.s. of Eq. (A7) corresponds to the order of magnitude  $\mu^0$ , the second one to  $\mu$ , and the last one to  $\mu^2$ . By substituting  $\tilde{p}(x)$  in the r.h.s. with  $\tilde{p}(x_0)$ , Eq. (A7) becomes a solution of Eq. (A4), approximated at the order  $\mu^2$ . Substituting Eq. (A4) in Eq. (A2) leads to

$$s(x) = \frac{1}{6\omega^2\rho_C} \text{Re} [ (1/2)(\beta+1)(2c+d)f_\nu \partial_x T_N |\partial_x \tilde{p}|^2 - k_C^2 (2cf_\nu + 3f_\nu^*) \tilde{p} \partial_x \tilde{p}^* ] + o(|f_\nu|). \quad (\text{A8})$$

Using the quantity  $R \equiv \tilde{p}^-( -H_S ) / \tilde{p}^+( -H_S )$  and using the lowest order of magnitude of Eqs. (1), (A6), and (A7), one can check that

$$\left| \frac{k_C^2 \tilde{p} \partial_x \tilde{p}^*}{\partial_x T_N |\partial_x \tilde{p}|^2} \right| \sim \left| \left( \frac{1+R}{1-R} \right) \frac{k_C T_N}{\partial_x T_N} \right| \sim \mu. \quad (\text{A9})$$

The second term in square brackets of Eq. (A8), proportional to the thickness  $\mu \ll 1$  of the stack, represents a small correction of the first one.

The porosity  $\phi < 1$  of the stack must now be considered. First, the hydrodynamic resistance of the stack increases by a factor  $(1/\phi)$ . The mass flux per unit area in the waveguide region is then

$$M(\phi < 1) = \phi M(\phi = 1). \quad (\text{A10})$$

Second, the acoustic pressure  $\tilde{p}(x)$  in the l.h.s. of Eqs. (A6) and (A7) represents the acoustic pressure inside the stack ( $-H_S < x < 0$ ), and the quantity

$$T_N(x) \partial_x \tilde{p}(x) \approx i \omega \rho_C \tilde{v}(x) + o(|f_\nu|^0), \quad (\text{A11})$$

is proportional to the particle velocity  $\tilde{v}(x)$ . Therefore, the porosity of the stack induces a jump of the acoustic pressure gradient at the extremity of the stack, the acoustic field being measured at  $x = -H_S - 0$  (just outside the left side of the stack)

$$\partial_x \tilde{p}(-H_S + 0) = (1/\phi) \partial_x \tilde{p}(-H_S - 0). \quad (\text{A12})$$

In Ref. 9, the stack is first assumed to be acoustically thin ( $\mu \ll 1$ ): contributions proportional to  $\mu$  are neglected in Eqs. (A6), (A7), and (A8). As a consequence, Eq. (A6) reduces to

$$T_N(x) \partial_x \tilde{p}(x) \approx (1/\phi) \partial_x \tilde{p}(-H_S) \approx (ik_C/\phi) \tilde{p}^+(1-R), \quad (\text{A13})$$

where the second line of Eq. (A13) has been derived using the expression of acoustic pressure defined in Eqs. (1) and (2) (neglecting terms proportional to  $|f_\nu|$ ). Finally, neglecting the anticlockwise wave compared to the clockwise one ( $|R| \ll 1$ ), the theoretical acoustically induced mass flux finally becomes

$$M_0 \approx \Delta |\tilde{p}^+|^2, \quad (\text{A14})$$

where the coefficient  $\Delta$  is given in Eq. (9). The theoretical mass flux  $M_0$  correspond to the one given in Ref. 9, subscript 0 indicating that Eq. (A14) is the theoretical value at the lowest order.

An improvement is derived by considering terms proportional to the length  $\mu$  of the stack, the anticlockwise wave still being neglected ( $|R| \ll 1$ ). Acoustic field is expressed at the necessary order of magnitude

$$p(x) \approx \tilde{p}^+, \quad (\text{A15})$$

$$T_N(x) \partial_x \tilde{p}(x) \approx (ik_C/\phi) \tilde{p}^+, \quad (\text{A16})$$

and the mass flux becomes

$$M_1 \approx (\Delta + \Delta') |\tilde{p}^+|^2, \quad (\text{A17})$$

where the coefficient  $\Delta'$  is given in Eq. (11). Subscript 1 indicates that Eq. (A17) corresponds to the improved theory.

Concerning the contribution of the anticlockwise wave, it would be possible to obtain a better estimation of the acoustically induced mass flux. Although this improvement is tractable, it is beyond the scope of our qualitative approach. In fact, taking into account the anticlockwise wave is not trivial because the experimental value of the ratio  $|R| \approx 0.47$  is close to the value of parameters  $\mu \approx 0.42$  and  $|f_\nu| \approx 0.37$ . This further improvement might introduce inaccurate correction terms of the order of magnitude of neglected terms  $|f_\nu| |R| \sim |f_\nu|^2 \ll |f_\nu|$  in  $M_0$  and  $\mu |f_\nu| |R| \sim |f_\nu|^3 \ll |f_\nu|$  in  $M_1$ . More accurate expressions of the density of streaming sources and of the acoustic field need to be considered at least by taking into account for terms proportional to  $|f_\nu|^2$ , respectively, in Eqs. (A2) and (A4).

- <sup>1</sup>N. Rott, "Thermoacoustics," *Adv. Appl. Mech.* **20**, 135–175 (1980).
- <sup>2</sup>P. H. Ceperley, "A pistonless Stirling engine—the traveling wave heat engine," *J. Acoust. Soc. Am.* **66**, 1508–1513 (1979).
- <sup>3</sup>T. Yazaki, A. Iwata, T. Maekawa, and A. Tominaga, "Traveling wave thermoacoustic engine in a looped tube," *Phys. Rev. Lett.* **81**, 3128–3132 (1998).
- <sup>4</sup>S. Backhaus and G. W. Swift, "A thermoacoustic Stirling engine," *Nature (London)* **399**, 335–338 (1999); "A thermoacoustic-Stirling heat engine: Detailed study," *J. Acoust. Soc. Am.* **107**, 3148–3166 (2000).
- <sup>5</sup>T. Yazaki, T. Biwa, and A. Tominaga, "A pistonless Stirling cooler," *Appl. Phys. Lett.* **80**, 157–159 (2002).
- <sup>6</sup>R. S. Reid, W. C. Wards, and G. W. Swift, "Cyclic thermodynamics with open flow," *Phys. Rev. Lett.* **80**, 4617–4620 (1998).
- <sup>7</sup>R. S. Reid and G. W. Swift, "Experiments with a flow-through thermoacoustic refrigerator," *J. Acoust. Soc. Am.* **108**, 2835–2842 (2000).
- <sup>8</sup>D. Gedeon, "DC gas flow in Stirling and pulse-tube cryocoolers," *Cryogenics* **9**, 385–392 (1997).
- <sup>9</sup>V. Gusev, S. Job, H. Bailliet, P. Lotton, and M. Bruneau, "Acoustic streaming in annular thermoacoustic prime-movers," *J. Acoust. Soc. Am.* **108**, 934–945 (2000).
- <sup>10</sup>G. W. Swift, "Thermoacoustic engines," *J. Acoust. Soc. Am.* **84**, 1145–1180 (1988).
- <sup>11</sup>J. R. Olsen and G. W. Swift, "Acoustic streaming in pulse tube refrigerators: Tapered pulse tubes," *Cryogenics* **37**, 769–776 (1998).
- <sup>12</sup>V. Gusev, H. Bailliet, P. Lotton, and M. Bruneau, "Asymptotic theory of nonlinear acoustic waves in a thermoacoustic prime-mover," *Acust. Acta Acust.* **86**, 25–38 (2000).
- <sup>13</sup>G. Penelet, E. Gaviot, V. Gusev, P. Lotton, and M. Bruneau, "Experimental investigation of transient nonlinear phenomena in an annular thermoacoustic prime-mover: Observation of a double-threshold effect," *Cryogenics* **42**, 527–532 (2002).
- <sup>14</sup>F. P. Incropera and D. P. De Witt, *Introduction to Heat Transfer*, 3rd ed. (Wiley, New York, 1996).
- <sup>15</sup>L. D. Landau and E. M. Lifshitz, *Fluid Mechanics* (Pergamon, Oxford, 1982).
- <sup>16</sup>H. Bailliet, V. Gusev, R. Raspet, and R. A. Hiller, "Acoustic streaming in closed thermoacoustic devices," *J. Acoust. Soc. Am.* **110**, 1808–1821 (2001).
- <sup>17</sup>F. M. White, *Fluid Mechanics*, 2nd ed. (McGraw-Hill, New York, 1986).